


RESEARCH ARTICLE | NOVEMBER 07 2022

A modified wall-adapting local eddy-viscosity model for large-eddy simulation of compressible wall-bounded flow

Han Qi (齐涵) ; Xinliang Li (李新亮) ; Changping Yu (于长平) 



Physics of Fluids 34, 116114 (2022)

<https://doi.org/10.1063/5.0119413>



View
Online



Export
Citation

CrossMark

Articles You May Be Interested In

Stochastic forcing for sub-grid scale models in wall-modeled large-eddy simulation

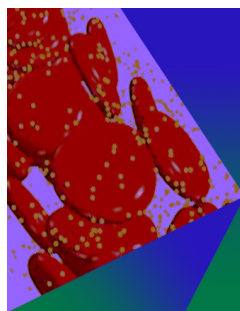
Physics of Fluids (September 2021)

A compressible wall-adapting similarity mixed model for large-eddy simulation of the impinging round jet

Physics of Fluids (March 2009)

A multiscale subgrid model for both free vortex flows and wall-bounded flows

Physics of Fluids (October 2009)



Physics of Fluids

Special Topic: Flow and Forensics

Submit Today!

 AIP
Publishing

 AIP
Publishing

A modified wall-adapting local eddy-viscosity model for large-eddy simulation of compressible wall-bounded flow

Cite as: Phys. Fluids **34**, 116114 (2022); doi: [10.1063/5.0119413](https://doi.org/10.1063/5.0119413)

Submitted: 9 August 2022 · Accepted: 16 October 2022 ·

Published Online: 7 November 2022






View Online



Export Citation



CrossMark

Han Qi (齐涵),^{1,2}  Xinliang Li (李新亮),^{1,2}  and Changping Yu (于长平)^{1,a)} 

AFFILIATIONS

¹LHD, Institute of Mechanics, Chinese Academy of Sciences, Beijing 100190, China

²School of Engineering Science, University of Chinese Academy of Sciences, Beijing 100049, China

^{a)} Author to whom correspondence should be addressed: cpyu@imech.ac.cn

ABSTRACT

The wall-adapting local eddy-viscosity (WALE) model in large-eddy simulation can well predict wall-bounded flows but it is also well known for excessive dissipation. In this study, we apply the minimum-dissipation model to constrain the WALE model in compressible flows and obtain the coefficient of the WALE model. Through this process, the dissipation of WALE model can be lower while it still maintains strong stability. In the modified WALE model, the isotropic part of the subgrid-scale (SGS) stress is also reconstructed. In the filtered total energy equation, all of the extra SGS unclosed terms (besides SGS stress and SGS heat flux) are modeled instead of neglecting some SGS terms, such as the SGS viscous diffusion. The modified WALE model is tested in a compressible turbulent channel flow and a supersonic turbulent boundary layer over a compression corner. The new model can well predict the mean velocity, the mean temperature, the Reynolds stress, and the separation bubble.

Published under an exclusive license by AIP Publishing. <https://doi.org/10.1063/5.0119413>

I. INTRODUCTION

Large-eddy simulation (LES) plays an increasingly important role in wall-bounded flow, especially at high Reynolds number turbulent flows. In LES, the filtered Navier–Stokes (N–S) equations have some subgrid-scale (SGS) terms, which should be modeled, and different kinds of SGS models are developed for simulating turbulent flows. The most popular SGS stress model is the eddy-viscosity model, which has strong numerical robustness and simplicity.¹ The Smagorinsky model (SM)^{2,3} is the most typical eddy-viscosity model and has been applied to different practical simulations. Then, many different eddy-viscosity models have been developed. Using a second-order structure function, Metals and Lesieur⁴ proposed a new SGS eddy viscosity. Nicoud and Ducros⁵ proposed the wall-adapting local eddy-viscosity (WALE) model, which can have the correct asymptotic behavior near the wall. Yet, the WALE model would supply excessive dissipation, and thus, some modified model for WALE has been proposed. Using the WALE operator, Bricteux *et al.*⁶ obtained a regularized variational multiscale model with the proper near-wall behavior. Lodato *et al.*⁷ developed a scale similarity version of the WALE model. There are also some other types of eddy-viscosity models. For obtaining good prediction of

turbulent shear flows, Vreman⁸ proposed a low dissipation eddy-viscosity model. Then, based on the singular values of the velocity gradient tensor, Nicoud *et al.*⁹ proposed the σ model, which can have good behavior for the wall-bounded shear flows. According to the balance of the helicity transfer and dissipation in the inertial region and a spectral relative helicity relation, Yu *et al.*¹⁰ supplied a new eddy-viscosity model, which was successfully applied to simulate compressible transitional flows.¹¹ Rozema *et al.*¹² supplied an anisotropic minimum-dissipation eddy-viscosity model, which does not need an approximation of the filter width. The SGS kinetic energy equation model (k -equation model) was also a type of eddy-viscosity model, which was introduced by Schumann¹³ through dimensional analysis for LES of incompressible flows. Yoshizawa¹⁴ also independently obtained the k -equation model from the two-scale direct interaction approximation. At the same time, the k -equation model was generalized to the compressible flows with the compressible effects considered in all the SGS terms,¹⁵ and the compressible k -equation model was also successfully applied to simulate the supersonic combustion flows.¹⁶ Subsequently, Chai and Mahesh¹⁷ proposed a new dynamic k -equation model for large-eddy simulation of compressible turbulence. In this new model, each of the unclosed quantities is modeled

independently instead of being grouped into production and dissipation terms. More recently, Qi *et al.*¹⁸ suggested a new one-equation model based on SGS helicity instead of SGS kinetic energy. The SGS helicity equation model is applied to the isotropic helical turbulence and incompressible turbulent channel flow, which can achieve more accurate predicted results.

In addition to the eddy-viscosity models, there are some other types of SGS models. Bardina *et al.*¹⁹ proposed the scale-similarity model and Liu *et al.*²⁰ revised it. By Taylor expansions for SGS stress, Clark *et al.*²¹ and Vreman *et al.*²² supplied the gradient model. Combining with the advantages of the SM and the scale-similarity model or the gradient model, several mixed models were proposed for improving the effects of LES.^{19,23–25} Under the assumption that the subgrid structure can be denoted by the resolved stretched vortices, Misra and Pullin²⁶ supplied a stretched-vortex SGS model, and then, it was extended to compressible flows.²⁷ Considering the joint probability function of the velocity, the velocity-filtered density-function-based SGS model was obtained by Gicquel *et al.*²⁸ Xie *et al.*²⁹ applied artificial neural network to nonlinear algebraic models for large eddy simulation of turbulence.

Many of the aforementioned SGS models are not very suitable for LES in compressible wall-bounded flows, and they need some modification or the dynamic procedure needs to be imposed to them.^{30–33} The dynamic procedure has challenges that arise in complex flows, such as the construction of test filters or the definition of homogeneous averaging operations.³⁴ In this paper, in order to obtain good prediction effects and avoid computational complexity, we propose a modified wall-adapting local eddy-viscosity model for compressible wall-bounded flows. In the new model, we use the minimum-dissipation eddy-viscosity model to constrain the WALE model which has correct behavior near the wall. Through this method, we can obtain proper dissipation and the new model can also have good behavior in the wall-bounded shear flows. The structure of this paper is as follows: LES governing equations and SGS models are introduced in Sec. II. The modified wall-adapting local eddy-viscosity model is supplied in Sec. III. In Sec. IV, the new model is tested in different testing cases. Finally, the conclusions are supplied in Sec. V.

II. LES GOVERNING EQUATIONS AND SUBGRID-SCALE MODELS

The filtered Navier–Stokes (N–S) equations for compressible flows in LES take the form

$$\frac{\partial \bar{\rho}}{\partial t} + \frac{\partial \bar{\rho} \tilde{u}_j}{\partial x_j} = 0, \tag{1}$$

$$\frac{\partial \bar{\rho} \tilde{u}_i}{\partial t} + \frac{\partial \bar{\rho} \tilde{u}_i \tilde{u}_j}{\partial x_j} = -\frac{\partial \bar{p}}{\partial x_i} + \frac{\partial \tilde{\sigma}_{ij}}{\partial x_j} - \frac{\partial \tau_{ij}}{\partial x_j}, \tag{2}$$

$$\begin{aligned} \frac{\partial \bar{\rho} \tilde{E}}{\partial t} + \frac{\partial (\bar{\rho} \tilde{E} + \bar{p}) \tilde{u}_j}{\partial x_j} = & -\frac{\partial \tilde{q}_j}{\partial x_j} + \frac{\partial \tilde{\sigma}_{ij} \tilde{u}_i}{\partial x_j} \\ & - \frac{\partial C_p Q_j}{\partial x_j} - \frac{\partial J_j}{\partial x_j} + H, \end{aligned} \tag{3}$$

where $(\bar{\cdot})$ represents spatial filtering with a low-pass filter at scale Δ and $(\tilde{\cdot})$ represents density-weighted (Favre) filtering ($\tilde{\phi} = \bar{\rho \phi} / \bar{\rho}$). In the filtered N–S equations, $\bar{\rho}$, \tilde{u}_i , \bar{p} , and \tilde{E} are the filtered density, velocity, pressure, and total energy, respectively.

In Eqs. (2) and (3), there are still some SGS unclosed terms, which are the SGS stress

$$\tau_{ij} = \bar{\rho} (\tilde{u}_i \tilde{u}_j - \tilde{u}_i \tilde{u}_j), \tag{4}$$

the SGS heat flux

$$Q_j = \bar{\rho} (\tilde{u}_j \tilde{T} - \tilde{u}_j \tilde{T}), \tag{5}$$

and the SGS turbulent diffusion term

$$J_j = \frac{1}{2} \bar{\rho} (\tilde{u}_i \tilde{u}_i \tilde{u}_j - \tilde{u}_i \tilde{u}_i \tilde{u}_j). \tag{6}$$

In this study, Eq. (3) is obtained by applying the filtering operator to the total energy equation, and the form of the filtered total energy can be represented as $\bar{\rho} \tilde{E} = \bar{\rho} C_v \tilde{T} + \frac{1}{2} \bar{\rho} \tilde{u}_i \tilde{u}_i + \frac{1}{2} \tau_{ii}$,¹⁷ where τ_{ii} is the isotropic part of SGS stress and can be expressed as

$$\tau_{ii} = \bar{\rho} (\tilde{u}_i \tilde{u}_i - \tilde{u}_i \tilde{u}_i). \tag{7}$$

In Eq. (3), the expression for H is

$$H = -\varepsilon_d + \frac{\partial}{\partial x_j} \left[\mu(\tilde{T}) \frac{\partial \frac{1}{2} \tau_{ii}}{\partial x_j} \right] + \frac{\partial}{\partial x_j} \left[\mu(\tilde{T}) \frac{\partial}{\partial x_i} \left(\frac{\tau_{ij}}{\bar{\rho}} \right) \right], \tag{8}$$

where ε_d is the dilatational dissipation and it can be expressed as

$$\varepsilon_d = \frac{\partial}{\partial x_j} \left[\frac{5}{3} (\mu(\tilde{T}) \tilde{u}_j \frac{\partial \tilde{u}_k}{\partial x_k} - \mu(\tilde{T}) \tilde{u}_j \frac{\partial \tilde{u}_k}{\partial x_k}) \right]. \tag{9}$$

The filtered pressure is determined by $\bar{p} = \bar{\rho} R \tilde{T}$, where R is the specific gas constant and \tilde{T} is the filtered temperature. The resolved viscous stress $\tilde{\sigma}_{ij}$ and heat flux \tilde{q}_j are expressed as

$$\tilde{\sigma}_{ij} = 2\mu(\tilde{T}) \tilde{S}_{ij}, \tag{10}$$

$$\tilde{S}_{ij} = \tilde{S}_{ij} - \frac{1}{3} \delta_{ij} \tilde{S}_{kk} = \frac{1}{2} \left(\frac{\partial \tilde{u}_i}{\partial x_j} + \frac{\partial \tilde{u}_j}{\partial x_i} \right) - \frac{1}{3} \frac{\partial \tilde{u}_k}{\partial x_k} \delta_{ij}, \tag{11}$$

$$\tilde{q}_j = -\frac{C_p \mu(\tilde{T})}{P_r} \frac{\partial \tilde{T}}{\partial x_j}, \tag{12}$$

where the molecular viscosity μ takes the form $\mu = \frac{1}{Re} \left(\frac{\tilde{T}}{T_\infty} \right)^{3/2} \frac{\tilde{T}_\infty + T_s}{T + T_s}$ according to Sutherland's law in which T_s is 110.3 K, the Reynolds number Re takes the form $Re = \rho_\infty U_\infty L / \mu_\infty$, and $\tilde{S}_{ij} = \frac{1}{2} \left(\frac{\partial \tilde{u}_i}{\partial x_j} + \frac{\partial \tilde{u}_j}{\partial x_i} \right)$ is the resolved strain-rate tensor. C_p is the specific heat at constant pressure and P_r is the molecular Prandtl number.

Because of its numerical robustness and simplicity, the eddy-viscosity model is most often adopted in practical simulations.^{1,12} The eddy-viscosity model is a phenomenological model, and the proposal of this model is based on the Boussinesq type hypothesis, which is

$$\tau_{ij}^{mod} - \frac{1}{3} \delta_{ij} \tau_{kk}^{mod} = -2\mu_{sgs} \tilde{S}_{ij}, \tag{13}$$

where τ_{kk}^{mod} is the isotropic part of the SGS stress model.

In the eddy-viscosity model, the SM is the typical model and widely exists in LES of different types of flows.² In the SM, the eddy viscosity can be written as

$$\mu_{sgs}^{mod} = \bar{\rho} (C_{sm} \Delta)^2 |\tilde{S}|, \quad (14)$$

where

$$\tilde{S} = \sqrt{2\tilde{S}_{ij}\tilde{S}_{ij}}, \quad (15)$$

and C_{sm} is the coefficient of the anisotropic part of the SM. The isotropic part of the SGS tensor for the SM is

$$\tau_{kk}^{mod} = 2C_I \bar{\rho} \Delta^2 |\tilde{S}|^2, \quad (16)$$

where C_I is the coefficient of the isotropic part of the SM.³⁵

In original WALE model, only the SGS viscosity is given as

$$\mu_{sgs}^w = \bar{\rho} C_w (\Delta)^2 \frac{(S_{ij}^d S_{ij}^d)^{3/2}}{(\tilde{S}_{ij} \tilde{S}_{ij})^{5/2} + (S_{ij}^d S_{ij}^d)^{5/4}} \quad (17)$$

with C_w is the coefficient of the WALE model and

$$S_{ij}^d = \frac{1}{2} \left(\frac{\partial \tilde{u}_i}{\partial x_j} + \frac{\partial \tilde{u}_j}{\partial x_i} \right) - \frac{1}{3} \frac{\partial \tilde{u}_m}{\partial x_m} \delta_{ij}. \quad (18)$$

For the SGS heat flux model, we take the commonly used SGS diffusion model³⁶ as

$$Q_j^{mod} = -\frac{\mu_{sgs}}{Pr_{sgs}} \frac{\partial \tilde{T}}{\partial x_j}, \quad (19)$$

where Pr_{sgs} is the SGS Prandtl number.

III. MODIFIED WALL-ADAPTING LOCAL EDDY-VISCOSITY (MWALE) MODEL

In this section, we will supply the derivation of the modified wall-adapting local eddy-viscosity (MWALE) model. First, we introduce the anisotropic minimum-dissipation (AMD) model to constrain the wall-adapting local (WALE) model to obtain proper SGS dissipation. The AMD model can be expressed as

$$\mu_{sgs}^{AMD} = \bar{\rho} C \frac{\max\{-(\Delta_k \partial_k \tilde{u}_i)(\Delta_k \partial_k \tilde{u}_j) \tilde{S}_{ij}, 0\}}{(\partial_l \tilde{u}_m)(\partial_l \tilde{u}_m)}, \quad (20)$$

where C is the coefficient of the AMD model and it is recommended as 0.3. Δ_k is the grid width in the x_k direction. Rozema *et al.*¹² demonstrated consistency of the AMD model with the exact kinetic energy flux. However, it has been shown that the AMD model has a singular eddy viscosity, which will lead to instability.³⁷ The WALE model shows good near-wall behavior and strong stability and has been applied in shock/boundary layer interaction successfully.³⁸ Thus, we choose the WALE model as the object model. We make $\mu_{sgs}^{AMD} = \mu_{sgs}^w$ to obtain proper SGS dissipation for WALE model. Then, we can obtain the coefficient C_w as

$$C_w = C \frac{\max\{-(\Delta_k \partial_k \tilde{u}_i)(\Delta_k \partial_k \tilde{u}_j) \tilde{S}_{ij}, 0\}}{\Delta^2 (S_{ij}^d S_{ij}^d)^{3/2} (\partial_l \tilde{u}_m)(\partial_l \tilde{u}_m)} \left[(\tilde{S}_{ij} \tilde{S}_{ij})^{5/2} + (S_{ij}^d S_{ij}^d)^{5/4} \right]. \quad (21)$$

Then, in order to well predict the compressible effect, we will model the isotropic part of SGS stress for MWALE model. Following the definition of the WALE model, the isotropic part of SGS stress for MWALE model can be expressed as

$$\tau_{kk}^w = 2C_{I,w} \bar{\rho} \Delta^2 \mu_{sgs}^w \frac{\partial \tilde{u}_k}{\partial x_k}, \quad (22)$$

where $C_{I,w}$ is the coefficient of the isotropic part of the MWALE model. The SGS stress model in the MWALE model can be written as

$$\tau_{ij}^{mod} = -2\mu_{sgs}^w \tilde{S}_{ij} + \frac{1}{3} \delta_{ij} \tau_{kk}^w. \quad (23)$$

To obtain an exact isotropic part of SGS stress for MWALE model in compressible flows, we introduced the infinite series expansion³⁹ to expand it. The infinite series expansion is expressed as

$$\begin{aligned} \bar{f}g - \bar{f}\bar{g} &= \alpha \frac{\partial \bar{f}}{\partial x_k} \frac{\partial \bar{g}}{\partial x_k} + \frac{1}{2!} (\alpha)^2 \frac{\partial^2 \bar{f}}{\partial x_k \partial x_l} \frac{\partial^2 \bar{g}}{\partial x_k \partial x_l} \\ &+ \frac{1}{3!} (\alpha)^3 \frac{\partial^3 \bar{f}}{\partial x_k \partial x_l \partial x_m} \frac{\partial^3 \bar{g}}{\partial x_k \partial x_l \partial x_m} + \dots, \end{aligned} \quad (24)$$

where

$$\alpha(y) = \int_{-\infty}^{\infty} 2x^2 G(x, y) dx. \quad (25)$$

Here, $G(x, y)$ is the kernel of the filter, and f and g can be vector or scalar. In this study, $G(x, y)$ is designated as the box filter for the case of *a priori* test and the grid filter⁴⁰ is used in the LES cases. α can be taken as $\alpha = C_0 \Delta_k^2$. When the box filter is applied, C_0 takes 1/12 and we take C_0 as 0.1 for practical simulations in this study.

By applying Eq. (24) to the isotropic part of SGS stress, τ_{kk} can be expanded as

$$\tau_{kk} = C_0 \Delta_l^2 \bar{\rho} \frac{\partial \tilde{u}_k}{\partial x_l} \frac{\partial \tilde{u}_k}{\partial x_l} + \frac{1}{2!} (C_0^2 \Delta_l^2 \Delta_m^2) \bar{\rho} \frac{\partial^2 \tilde{u}_k}{\partial x_l \partial x_m} \frac{\partial^2 \tilde{u}_k}{\partial x_l \partial x_m} + \dots \quad (26)$$

For avoiding the complexity of additional boundary conditions and considering the other higher-order terms are small enough compared to the first term of Eq. (26), we keep the first term of Eq. (26) as the modeled τ_{kk}

$$\tau_{kk}^{mod} = C_0 \Delta_l^2 \bar{\rho} \frac{\partial \tilde{u}_k}{\partial x_l} \frac{\partial \tilde{u}_k}{\partial x_l}. \quad (27)$$

Make $\tau_{kk}^{mod} = \tau_{kk}^w$ and the coefficient $C_{I,w}$ can be written as

$$C_{I,w} = \frac{C_0 \Delta_l^2 (\partial_l \tilde{u}_k)(\partial_l \tilde{u}_k)}{2\Delta^2 \mu_{sgs}^w \tilde{S}_{kk}}. \quad (28)$$

TABLE I. The grid setting and grid resolutions of the simulations in compressible turbulent channel flow.

Case	Grids	Δx^+	Δy_{min}^+	Δz^+
DNS	900 × 201 × 300	2.99	0.32	2.99
LES	48 × 65 × 48	57.5	1.07	19.18

TABLE II. The main parameters for the simulations in the compressible turbulent channel flow.

	Re_τ	Ma_τ	$-B_q$	u_c/U_m	ρ_c/ρ_w	T_c/T_w
DNS	220	0.0815	0.0445	1.156	0.717	1.388
DSM	208	0.0804	0.0429	1.158	0.719	1.373
WALE	204	0.0771	0.0422	1.159	0.717	1.390
MWALE	218	0.0817	0.0447	1.155	0.718	1.387

In the filtered total energy equation, there are some unclosed terms which need to be modeled. For the SGS turbulent diffusion term, we can model it as $J_j = \tau_{ij} \tilde{u}_i$.⁴¹ Similar to the isotropic part of SGS stress, the dilatational dissipation term ε_d can also be modeled as

$$\varepsilon_d \approx \frac{5}{3} \frac{\partial}{\partial x_j} \left[C_0 \Delta_l^2 \mu(\tilde{T}) \frac{\partial \tilde{u}_j}{\partial x_l} \frac{\partial^2 \tilde{u}_k}{\partial x_k \partial x_l} \right], \quad (29)$$

where the coefficient C_0 takes same value with Eq. (28).

For the SGS heat flux model, we choose the form in Eq. (19) and the SGS Prandtl number Pr_{sgs} is given by 0.9 in the following. Thus far, we have obtained all the unclosed terms in the filtered N-S equations [Eqs. (1)–(3)] and the MWALE model has been completed. Next, we will test and analyze the proposed model in different cases of compressible wall-bounded flows.

IV. NUMERICAL RESULTS AND ANALYSIS

In the following, we will first test the MWALE model in the compressible turbulent channel flow, which is a typical wall-bounded flow. Then, the new model will be tested in a supersonic turbulent boundary layer over a compression corner, which contains shock wave/turbulent boundary layer interaction and separation.

A. Compressible turbulent channel flow

In this section, a fully developed compressible turbulent channel flow^{42,43} is selected as the first test case for MWALE. Regarding the compressible turbulent channel flow, the size of the computational domain is $L_x \times L_y \times L_z = 4\pi \times 2 \times 4\pi/3$, the Mach number is $M_a = 1.5$, the bulk Reynolds number Re is 3000, the friction Reynolds number $Re_\tau = u_\tau \delta / \nu$ is 220 ($u_\tau = \sqrt{\tau_w / \rho_w}$ is the friction velocity, τ_w is the wall shear stress, ρ_w is the wall density, δ is the channel half-width, and ν is the kinematic viscosity; $Re_\tau = 220$ is the result of the simulations), the friction Mach number $Ma_\tau = u_\tau / a_w$ is

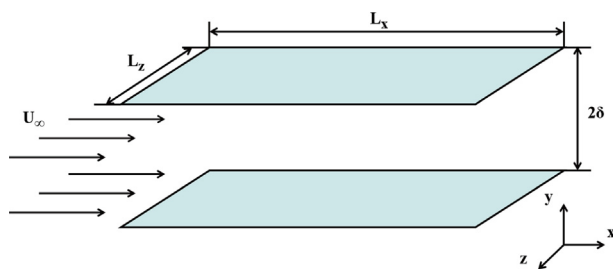


FIG. 1. Schematic diagram for the compressible turbulent channel flow.

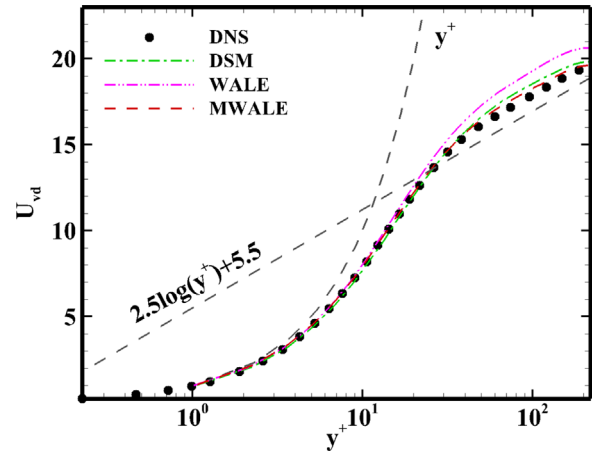


FIG. 2. The profile of the Van Driest transformed mean velocity U_{vd} from different SGS models and DNS.

approximately 0.0815 (a_w is the sound speed based on the wall temperature), the Prandtl number $Pr = \mu C_p \kappa$ is 0.7 (κ is the thermal conductivity, and C_p is the specific heat at constant pressure), and the ratio of specific heats is $\gamma = C_p / C_v = 1.4$ (C_v is the specific heat at constant volume). The flow is driven by a uniform body force. Periodic boundary conditions are applied in the streamwise and spanwise directions. The nonslip boundary condition and isothermal-wall boundary conditions are utilized on the walls. For LES, the filtered Navier–Stokes equations are solved using a high-precision nondimensional finite difference solver in Cartesian coordinates. In this solver, a sixth-order central difference scheme is applied to discretize both the convective and viscous terms, and the third-order Runge–Kutta scheme is used for the time advance. The dynamic Smagorinsky model (DSM) and the WALE model are compared with the new model. A box filter is used for test filtering for the Germano identity of the dynamic procedure, where the test-filter width is 2Δ ($\Delta = (\Delta_x \Delta_y \Delta_z)^{1/3}$). Tables I and II show the grid settings and main

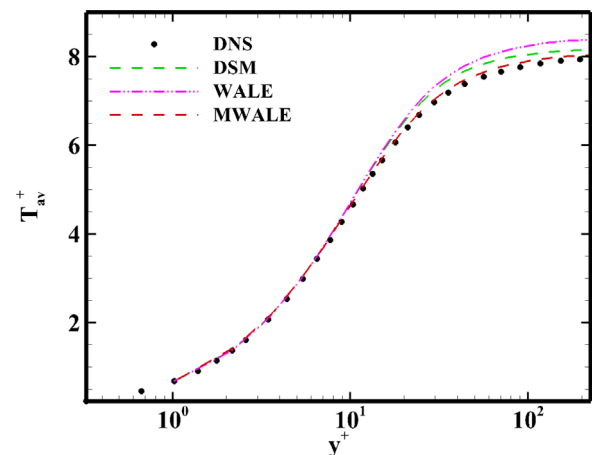


FIG. 3. The profiles of the mean temperature T_{av}^+ from different SGS models and DNS.

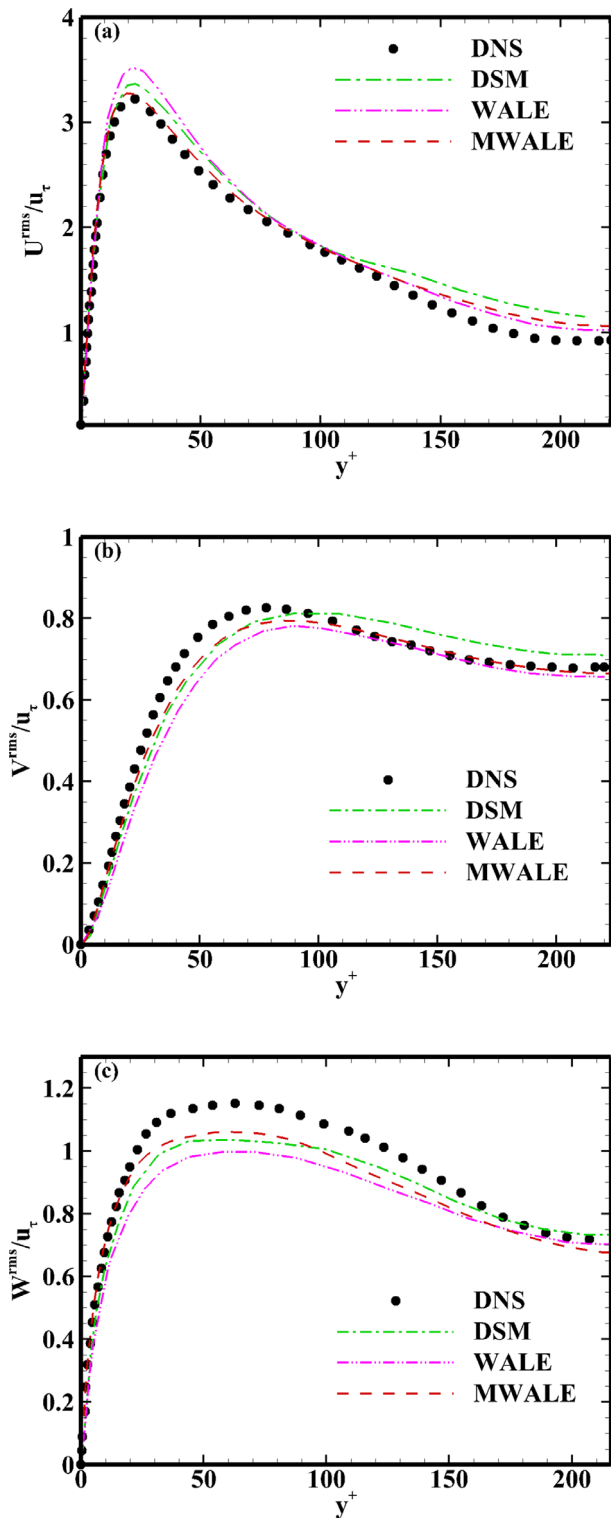


FIG. 4. The profiles of the resolved turbulence intensities normalized by the friction velocity u_τ from different SGS models and DNS: (a) streamwise turbulence intensity, (b) wall-normal turbulence intensity, and (c) spanwise turbulence intensity.

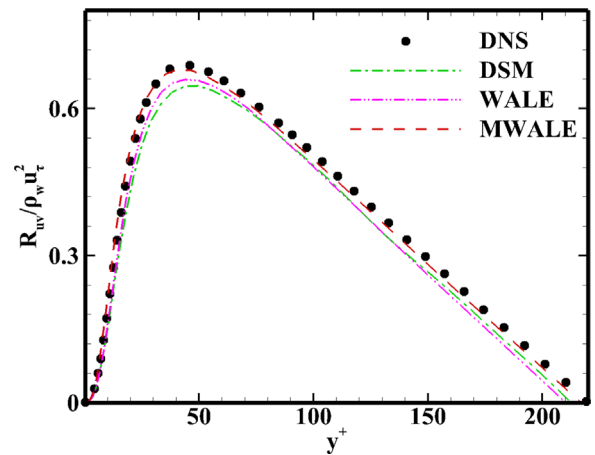


FIG. 5. The profiles of the total Reynolds stress normalized by ρ_w and u_τ from different SGS models and DNS.

parameters for DNS and LES in this case, respectively (u_c , ρ_c and T_c are the streamwise velocity, density, and temperature at the midplane of the channel flow). Figure 1 shows a schematic diagram of the compressible turbulent channel flow.

Figure 2 shows the profile of the Van Driest transformed mean velocity ($U_{vd} = \int_0^U \sqrt{\langle \rho \rangle} / \rho_w d(U)$) from different SGS models and DNS. From the figure, we know that the MWALE model can have good prediction and have better results than the DSM and WALE model. Figure 3 shows the profiles of the mean temperature $T_{av}^+ = (T_w - \langle T \rangle) / T_\tau$ from different SGS models and DNS [$T_\tau = B_q T_w$ is the friction temperature, $B_q = q_w / (\rho_w c_p u_\tau T_w)$ is the nondimensional heat flux, and q_w is the wall-normal heat flux]. In this figure, the MWALE model have obvious improvement contrast with the WALE model and the MWALE model have better behavior than the DSM.

Next, we show the profiles of the resolved turbulence intensities normalized by the friction velocity u_τ from different SGS models and DNS in Fig. 4. Figure 4(a) shows the streamwise turbulence intensity

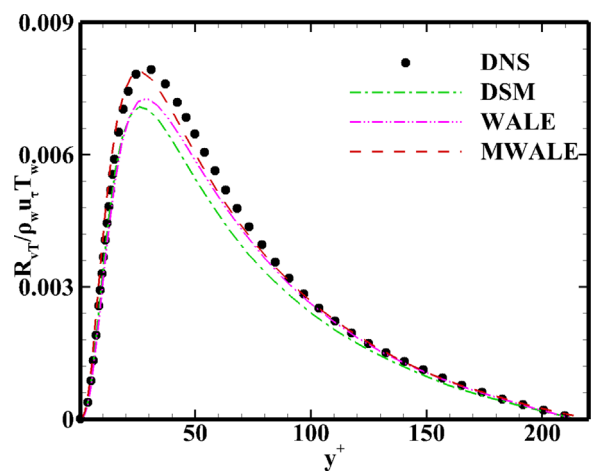


FIG. 6. The profiles of the turbulent heat flux normalized by ρ_w , u_τ , and T_w from different SGS models and DNS.

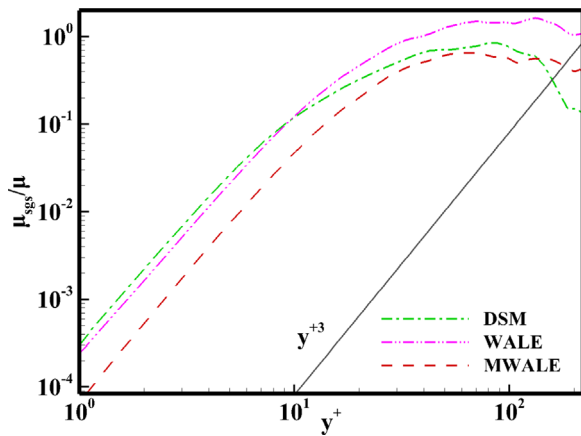


FIG. 7. Averaged SGS eddy viscosity $\langle \mu_{sgs} \rangle$ (normalized by μ) from different SGS models of the turbulent channel flow.

and the MWALE model can have best performance at almost regions. Figure 4(b) shows the wall-normal turbulence intensity. The MWALE model and DSM have almost same behavior at $0 < y < 80$ and their results are better than that of the WALE model. At $100 < y < 220$, the MWALE model and WALE model have good prediction. Overall, the MWALE model predicts best than other SGS models. Figure 4(c) shows spanwise turbulence intensity. In this figure, the MWALE model have best prediction at $0 < y < 100$. The DSM behaves best at $100 < y < 180$ while the MWALE model also have proper results. From the figures, we know that the MWALE model have obvious improvement compared with the WALE model.

For further investigating the predicting effects of the MWALE model, we show the profiles of the total Reynolds stress normalized by $\rho_w u_\tau$, and the turbulent heat flux normalized by $\rho_w u_\tau$, and T_w from different SGS models and DNS in Figs. 5 and 6. The total Reynolds stress could be expressed as

$$R_{ij} = \langle \bar{\rho} \rangle (\{ \widetilde{u_i u_j} \} - \{ \widetilde{u_i} \} \{ \widetilde{u_j} \}) = R_{ij}^{LES} + \langle \tau_{ij} \rangle, \quad (30)$$

where

$$R_{ij}^{LES} = \langle \bar{\rho} \rangle (\{ \widetilde{u_i u_j} \} - \{ \widetilde{u_i} \} \{ \widetilde{u_j} \}), \quad (31)$$

is the resolved Reynolds stress, and $\{ \cdot \}$ denotes the Favre averaging $(\{ \phi \} = \frac{\langle \rho \phi \rangle}{\langle \rho \rangle})$. The turbulent heat flux takes the form

$$R_{u_j T} = \langle \bar{\rho} \rangle (\{ \widetilde{u_j T} \} - \{ \widetilde{u_j} \} \{ \widetilde{T} \}) = R_{u_j T}^{LES} + \langle Q_j \rangle, \quad (32)$$

where

$$R_{u_j T}^{LES} = \langle \bar{\rho} \rangle (\{ \widetilde{u_j T} \} - \{ \widetilde{u_j} \} \{ \widetilde{T} \}), \quad (33)$$

TABLE III. The grid setting and grid resolutions of the simulations in compressible turbulent channel flow ($Ma = 3.0$ and $Re = 4880$).

Case	Grids	Δx^+	Δy_{min}^+	Δz^+
LES	$86 \times 97 \times 86$	66.4	1.44	22.14

TABLE IV. The main parameters for the simulations in the compressible turbulent channel flow ($Ma = 3.0$ and $Re = 4880$).

	Re_τ	Ma_τ	$-B_q$	u_c/U_m	ρ_c/ρ_w	T_c/T_w
DSM	444	0.101	0.125	1.21	0.399	2.69
WALE	436	0.099	0.121	1.22	0.397	2.70
MWALE	449	0.109	0.129	1.16	0.391	2.62

is the resolved turbulent heat flux. From the figures, we know that the MWALE model can have almost perfect prediction at all the regions. The WALE model can also have better results than the DSM.

To see the behavior near the wall of different SGS models, we show averaged SGS eddy viscosity $\langle \mu_{sgs} \rangle$ (normalized by μ) from different SGS models in Fig. 7. From the figure, we can know that the

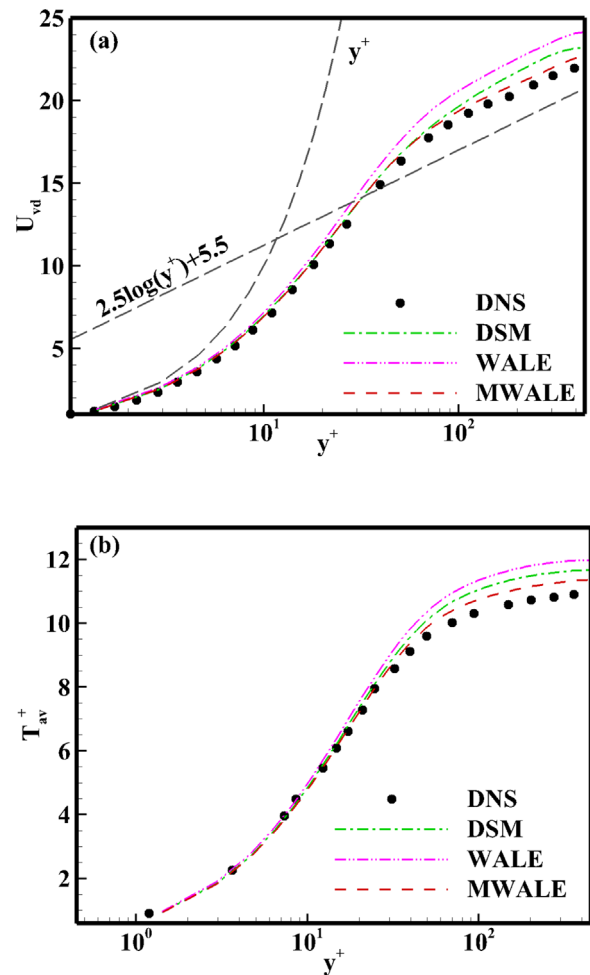


FIG. 8. The profiles of the Van Driest transformed mean velocity U_{vd} and the mean temperature T_{av}^+ at $Ma = 3.0$ and $Re = 4880$ from different SGS models and DNS: (a) mean velocity and (b) mean temperature. The DNS results are from Coleman et al.⁴².

TABLE V. The grid setting and grid resolutions of the simulations in supersonic turbulent boundary layer over a compression corner.

Case	Grids	$\Delta x^+(x = -335)$	$\Delta x^+(x \geq -35)$	Δy_{min}^+	Δz^+
DNS	$4000 \times 160 \times 200$	6.52	2.90	0.58	4.06
LES	$540 \times 100 \times 40$	40.60	40.60	0.87	20.30

wall scaling satisfies $O(y^{+3})$ at $y^+ < 20$ for WALE and MWALE model. The DSM follows the wall scaling ($O(y^{+3})$) at $y^+ < 10$. In general, the SGS eddy viscosity from MWALE is lower than these from the DSM and WALE model, and the value of SGS eddy viscosity from WALE is highest.

To test the new model in the case of a higher Reynolds number, we will discuss the results for the case of $Ma = 3.0$ and $Re = 4880$, where Re_τ is 451. The size of the computational domain, the boundary conditions, the ratio of specific heats, the Prandtl number Pr , and the setting of LES solver are all same with the case of $Ma = 1.5$ and $Re = 3000$. The grid setting and grid resolutions of the simulations in the compressible turbulent channel flow of this case are listed in Table III. Table IV gives the main parameters for the simulations in the compressible turbulent channel flow.

Figure 8 shows the profiles of the Van Driest transformed mean velocity U_{vd} and the mean temperature T_{av}^+ at $Ma = 3.0$ and $Re = 4880$ from different SGS models and DNS. From the results, we know that the MWALE model also shows better predictions than the DSM and WALE model at higher Reynolds number.

From the key quantities of the compressible channel flow, we know that the MWALE model has a significant improvement. Next, we will test the new model in the supersonic turbulent boundary layer over a compression corner.

B. Supersonic turbulent boundary layer over a compression corner

In this section, we will test the new model in the supersonic turbulent boundary layer over a 24° compression corner, which contains the transition process and the separation. The same example can be seen in the research works of Bookey *et al.*,⁴⁴ and Wu and Martin.⁴⁵ Steady laminar boundary layer profiles are imposed at the inlet, nonreflecting boundary conditions are applied in the outlet, the no-slip condition is used in the wall, nonreflecting boundary conditions are used at the top boundary, and the periodic condition is applied in the spanwise direction. The computational domains are $0 \leq y \leq 35$ mm in the wall-normal direction and $0 \leq z \leq 14$ mm in the spanwise direction, and the stream domain is $-335 \leq x \leq 49.56$ mm. The blowing and suction perturbation on the wall in $-305 \leq x \leq -285$ mm is imposed to trigger the bypass-type transition, and then the flow develops to

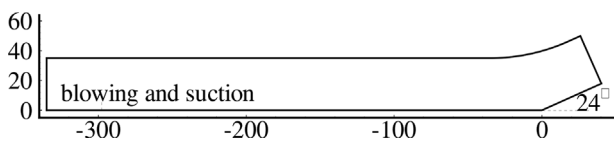


FIG. 9. Schematic diagram for the supersonic turbulent boundary layer over a compression corner.

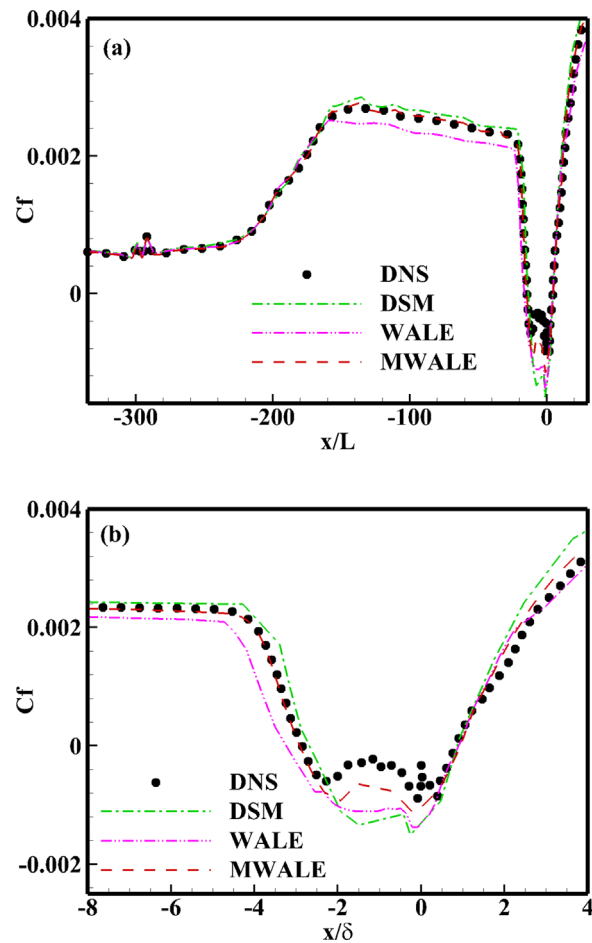


FIG. 10. Distribution of the skin-friction coefficient from different SGS models and DNS. (a) Distribution of the skin-friction coefficient along the streamwise direction and (b) distribution of the skin friction coefficient in the corner region, where the horizontal coordinates are normalized by the boundary-layer thickness δ .

turbulence. The full developed incoming turbulent boundary layer is generated via the laminar-to-turbulent transition method. Similar method can be found in some research.⁴⁶ L (one mm) is the non dimensionalizing length scale. The freestream Mach number $Ma_\infty = 2.9$, the freestream unit Reynolds number $Re/mm = 5581.4$, and the freestream temperature is 108.1 K. The convective and viscous terms are discretized by a sixth-order central difference scheme, and the third-order Runge-Kutta scheme is used for the time advance. Table V shows the grid-setting and main parameters of the simulations in supersonic turbulent boundary layer over a compression corner. Figure 9 shows schematic diagram for the supersonic turbulent boundary layer over a compression corner.

Figure 10(a) shows distribution of the skin-friction coefficient ($C_f = \tau_w / (\rho_\infty U_\infty^2 / 2)$) along the streamwise direction from SGS models and DNS. This figure shows that C_f has a drastic increase near the region $x = -200$ mm, which denotes the occurrence of transition (this transition type here is bypass transition apparently). From the figure, we know that the MWALE can well predict the transition process

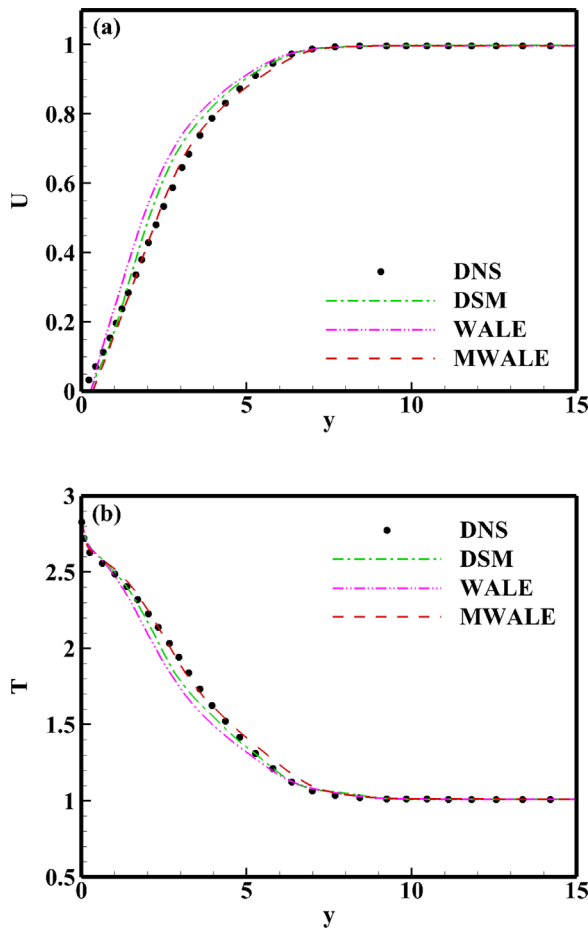


FIG. 11. The profiles of the streamwise velocity and the temperature at $x/\delta = -1$ from different SGS models and DNS: (a) streamwise velocity and (b) temperature.

in the case of bypass-type transition. In the corner region ($-35 < x < 35$ mm), the skin friction coefficient C_f goes down rapidly downstream and then shows a negative value, indicating that the separation occurs here. The skin friction coefficient C_f goes up rapidly and shows positive value again at $x = 0$ mm, indicating the reattachment of the flow. At that region, Fig. 10(a) cannot show the difference of SGS models. Thus, in order to carefully compare the performances of each model in the separation flow, distributions of the skin friction coefficient in the corner region from SGS models and DNS are shown in Fig. 10(b) (δ is the boundary-layer thickness). As shown in Fig. 10(b), the MWALE can well predict the separation, the reattachment, and the separation bubble.

Figure 11 shows the profiles of the streamwise velocity and the temperature at $x/\delta = -1$ from different SGS models and DNS, and the separation occurred in the region ($x/\delta = -1$). From the figures, we know that the MWALE can better predict the streamwise velocity and temperature than other SGS models. Figure 12 displays the profiles of the streamwise velocity and the temperature at $x/\delta = 1$, where the reattachment has happened. In the figures, all the SGS models can have good behavior and the results from the MWALE model are closer to the DNS results than other models.

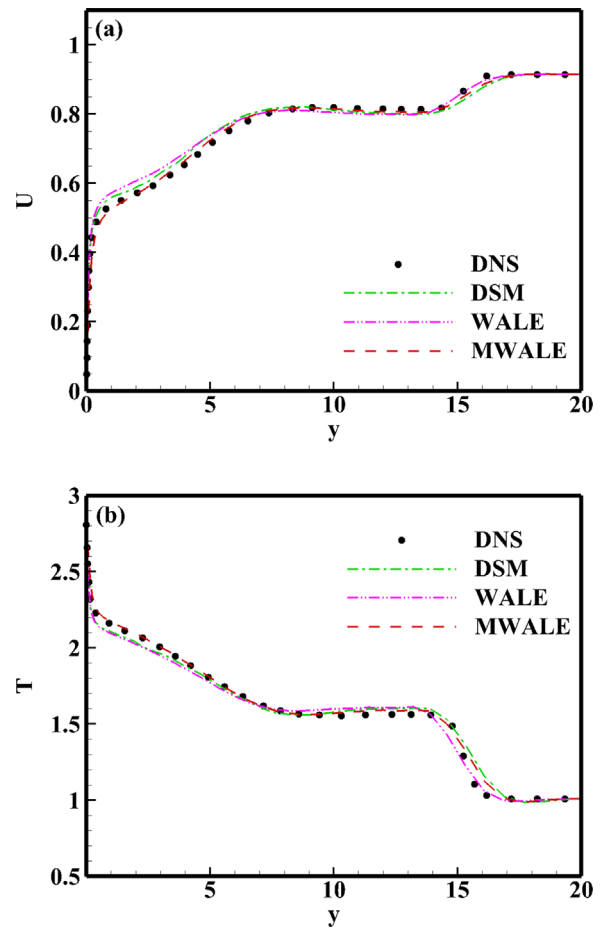


FIG. 12. The profiles of the streamwise velocity and the temperature at $x/\delta = 1$ from different SGS models and DNS: (a) streamwise velocity and (b) temperature.

V. CONCLUSION AND DISCUSSION

In this paper, we propose a modified wall-adapting local eddy-viscosity (MWALE) model for large-eddy simulation (LES) of compressible wall-bounded flow. In this new model, the minimum-dissipation model is applied to constrain the wall-adapting eddy-viscosity (WALE) model for obtaining lower SGS dissipation. The isotropic part of the SGS stress is reconstructed by maintaining the first term of the expanded term from the infinite series expansion. In the filtered total energy equation, the extra subgrid-scale (SGS) terms (besides SGS stress and SGS heat flux) are modeled using the same expanded method. The new model is tested in compressible turbulent channel flow and a supersonic turbulent boundary layer over a compression corner. It shows that the new model can have obvious improvement compared with the WALE model and also show better behaviors than the dynamic Smagorinsky model, including the mean velocity profile, the mean temperature profile, the RMS quantities, the total Reynolds stress, the turbulent heat flux, and the skin-friction coefficient, etc. Compared to the WALE model, the MWALE model can obtain precise kinetic energy flux and is also convenient to be applied in engineering.

In summary, the newly proposed model has strong stability and proper SGS dissipation, and it can also have correct behavior in the wall-bounded turbulence. In future research works, the new model will be applied to high Mach number flows in complex geometries.

ACKNOWLEDGMENTS

This work was supported by the National Key Research and Development Program of China (Grant Nos. 2020YFA0711800 and 2019YFA0405302) and NSFC Projects (Nos. 12072349, 91852203, 12072349, and 12202457), National Numerical Windtunnel Project, Science Challenge Project (Grant No. TZ2016001), and Strategic Priority Research Program of Chinese Academy of Sciences (Grant No. XDC01000000). The authors thank the National Supercomputer Center in Tianjin (NSCC-TJ) and the National Supercomputer Center in GuangZhou (NSCC-GZ) for providing computer time.

AUTHOR DECLARATIONS

Conflict of Interest

The authors have no conflicts to disclose.

Author Contributions

Han Qi: Conceptualization (equal); Data curation (equal); Investigation (equal); Methodology (equal); Software (equal); Validation (equal); Writing – original draft (equal). **Xinliang Li:** Funding acquisition (equal); Project administration (equal); Resources (lead); Software (lead); Supervision (equal). **Changping Yu:** Data curation (equal); Investigation (equal); Methodology (equal); Resources (equal); Validation (equal); Writing – original draft (equal); Writing – review & editing (equal).

DATA AVAILABILITY

The data that support the findings of this study are available from the corresponding author upon reasonable request.

REFERENCES

- C. Meneveau and J. Katz, "Scale-invariance and turbulence models for large-eddy simulation," *Annu. Rev. Fluid Mech.* **32**, 1–32 (2000).
- J. Smagorinsky, "General circulation experiments with the primitive equations: I. The basic experiment," *Mon. Weather Rev.* **91**, 99–164 (1963).
- D. K. Lilly, "On the application of the eddy viscosity concept in the inertial sub-range of turbulence," *NCAR Manuscript* (1967), p. 123.
- O. Metais and M. Lesieur, "Spectral large-eddy simulation of isotropic and stably stratified turbulence," *Annu. Rev. Fluid Mech.* **239**, 157–194 (1992).
- F. Nicoud and F. Ducros, "Subgrid-scale stress modelling based on the square of the velocity gradient tensor," *Flow, Turbul. Combust.* **63**, 183–200 (1999).
- M. D. L. Bricteux and G. Winckelmans, "A multiscale subgrid model for both free vortex flows and wall-bounded flows," *Phys. Fluids* **21**, 105102 (2009).
- G. Lodato, L. V. Vervisch, and P. Domingo, "A compressible wall-adapting similarity mixed model for large-eddy simulation of the impinging round jet," *Phys. Fluids* **21**, 035102 (2009).
- A. W. Vreman, "An eddy-viscosity subgrid-scale model for turbulent shear flow: Algebraic theory and applications," *Phys. Fluids* **16**, 3670–3681 (2004).
- F. Nicoud, H. B. Toda, O. Cabrit, S. Bose, and J. Lee, "Using singular values to build a subgrid-scale model for large-eddy simulations," *Phys. Fluids* **23**, 085106 (2011).
- C. Yu, R. Hong, Z. Xiao, and S. Chen, "Subgrid-scale eddy viscosity model for helical turbulence," *Phys. Fluids* **25**, 095101 (2013).
- H. Zhou, X. Li, H. Qi, and C. Yu, "Subgrid-scale model for large-eddy simulation of transition and turbulence in compressible flows," *Phys. Fluids* **31**, 125118 (2019).
- W. Rozema, J. B. Hyun, M. Parviz, and V. Roel, "Minimum-dissipation models for large-eddy simulation," *Phys. Fluids* **27**, 085107 (2015).
- U. Schumann, "Subgrid scale model for finite difference simulations of turbulent flows in plane channels and annuli," *J. Comput. Phys.* **18**, 376–404 (1975).
- H. K. Yoshizawa, "A statistically-derived subgrid-scale kinetic energy model for the large-eddy simulation of turbulent flows," *J. Phys. Soc. Jpn.* **54**, 2834–2839 (1985).
- N. Patel, C. Stone, and S. Menon, "Large-eddy simulation of turbulent flow over an axisymmetric hill," AIAA Paper No.2003-976, 2003.
- F. Genin and S. Menon, "Dynamics of sonic jet injection into supersonic cross-flow," *J. Turbul.* **11**, N4 (2010).
- X. Chai and K. Mahesh, "Dynamic τ -equation model for large-eddy simulation of compressible flows," *J. Fluid Mech.* **699**, 385–413 (2012).
- H. Qi, X. Li, and C. Yu, "Subgrid-scale helicity equation model for large-eddy simulation of turbulent flows," *Phys. Fluids* **33**, 035128 (2021).
- J. Bardina, J. H. Ferziger, and W. C. Reynolds, "Improved turbulence models based on large-eddy simulation of homogeneous incompressible turbulent flows," Report No. TF-19 (Department of Mechanical Engineering, Stanford, 1984).
- S. Liu, C. Meneveau, and J. Katz, "On the properties of similarity subgrid-scale models as deduced from measurements in a turbulent jet," *J. Fluid Mech.* **275**, 83–119 (1994).
- R. A. Clark, J. H. Ferziger, and W. C. Reynolds, "Evaluation of subgrid-scale models using an accurately simulated turbulent flow," *J. Fluid Mech.* **91**, 1–16 (1979).
- B. Vreman, B. Geurts, and H. Kuerten, "Large-eddy simulation of the temporal mixing layer using the Clark model," *Theor. Comput. Fluid Dyn.* **8**, 309–324 (1996).
- Y. Zang, R. Street, and J. Koseff, "A dynamic mixed subgrid-scale model and its application to turbulent recirculating flows," *Phys. Fluids A* **5**, 3186–3196 (1993).
- B. Vreman, B. Geurts, and H. Kuerten, "On the formulation of the dynamic mixed subgrid-scale model," *Phys. Fluids* **6**, 4057–4059 (1994).
- K. Horiti, "A new dynamic two-parameter mixed model for large-eddy simulation," *Phys. Fluids* **9**, 3443–3464 (1997).
- A. Misra and D. Pullin, "A vortex-based subgrid stress model for large-eddy simulation," *Phys. Fluids* **9**, 2443–2454 (1997).
- B. Kosovic, D. Pullin, and R. Samtaney, "Subgrid-scale modeling for large-eddy simulations of compressible turbulence," *Phys. Fluids* **14**, 1511–1522 (2002).
- L. Gicquel, P. Givi, F. Jaber, and S. Pope, "Velocity filtered density function for large eddy simulation of turbulent flows," *Phys. Fluids* **14**, 1196–1213 (2002).
- C. Xie, Z. Yuan, and J. Wang, "Artificial neural network-based nonlinear algebraic models for large eddy simulation of turbulence," *Phys. Fluids* **32**, 115101 (2020).
- M. Germano, U. Piomelli, P. Moin, and W. Cabot, "A dynamic subgrid-scale eddy viscosity model," *Phys. Fluids A* **3**, 1760–1765 (1991).
- S. Ghosal, T. S. Lund, P. Moin, and K. Akselvoll, "A dynamic localization model for large-eddy simulation of turbulent flows," *J. Fluid Mech.* **286**, 229–255 (1995).
- C. Ronchi, M. Ypma, and V. M. Canuto, "On the application of the Germano identity to subgrid-scale modeling," *Phys. Fluids A* **4**, 2927–2929 (1992).
- V. Wong, "A proposed statistical-dynamic closure method for the linear or nonlinear subgrid-scale stress," *Phys. Fluids A* **4**, 1080–1082 (1992).
- R. Agrawal, M. P. Whitmore, K. P. Griffin, S. T. Bose, and P. Moin, "Non-Boussinesq subgrid-scale model with dynamic tensorial coefficients," *Phys. Rev. Fluids* **7**, 074602 (2022).
- A. Yoshizawa, "Statistical theory for compressible turbulent shear flows, with the application to subgrid modeling," *Phys. Fluids* **29**, 2152–2271 (1986).
- P. Moin, K. Squires, W. Cabot, and S. Lee, "A dynamic subgrid-scale model for compressible turbulence and scalar transport," *Phys. Fluids A* **3**, 2746–2757 (1991).

- ³⁷W. Rozema, H. J. Bae, and R. W. C. P. Verstappen, “Local dynamic gradient Smagorinsky model for large-eddy simulation,” *Phys. Rev. Fluids* **7**, 074604 (2022).
- ³⁸C. Wollblad, L. Davidson, and L.-E. Eriksson, “Large eddy simulation of transonic flow with shock wave/turbulent boundary layer interaction,” *AIAA J.* **44**, 2340–2353 (2006).
- ³⁹K. Bedford and W. Yeo, “Conjunctive filtering procedures surface water flow transport,” in *Large Eddy Simulation of Complex Engineering and Geophysical Flows*, edited by B. Galperin and S. A. Orszag (Cambridge University Press, 1993), pp. 513–537.
- ⁴⁰A. E. Tejada-Martínez and K. E. Jansen, “A dynamic Smagorinsky model with dynamic determination of the filter width ratio,” *Phys. Fluids* **16**, 2514–2528 (2004).
- ⁴¹M. P. Martín, U. Piomelli, and G. V. Candler, “Subgrid-scale models for compressible large-eddy simulation,” *Theor. Comput. Fluid Dyn.* **13**, 361–376 (2000).
- ⁴²G. N. Coleman, J. Kim, and R. D. Moser, “A numerical study of turbulent supersonic isothermal-wall channel flow,” *J. Fluid Mech.* **305**, 159–183 (1995).
- ⁴³Y. Morinishi, S. Tamano, and K. Nakabayashi, “Direct numerical simulation of compressible turbulent channel flow between adiabatic and isothermal walls,” *J. Fluid Mech.* **502**, 273–308 (2004).
- ⁴⁴P. Bookey, C. Wyckham, A. Smits, and P. Martin, “New experimental data of STBLI at DNS/LES accessible Reynolds numbers,” AIAA Paper No. AIAA-2005-309, 2005.
- ⁴⁵M. Wu and M. P. Martin, “Direct numerical simulation of supersonic turbulent boundary layer over a compression ramp,” *AIAA J.* **45**, 879–889 (2007).
- ⁴⁶J. Duan, X. Li, X. Li, and H. Liu, “Direct numerical simulation of a supersonic turbulent boundary layer over a compression-decompression corner,” *Phys. Fluids* **33**, 065111 (2021).